Proceedings World Geothermal Congress 2020+1
Reykjavik, Iceland, April - October 2021

Energy Balance Analysis of Hydraulic Fracturing During EGS Development

Tamaki Ishikawa and Koichi Yamada

Science Plaza 4F, Yonbancho 5-3, Chiyodaku, Tokyo, 102-8666, Japan

ishikawa@jst-lcs.jp

Keywords: hydraulic fracturing, induced earthquake, energy balance, enhanced geothermal system

ABSTRACT

The magnitude of induced earthquakes is determined by the pressure and flow rate of the injected water and the subsurface structure during hydraulic fracturing for development of Enhanced Geothermal System (EGS). The relationship between hydraulic fracturing and induced earthquakes needs to be quantified in order to reduce induced earthquakes. In this paper the energy balance of hydraulic fracturing is analyzed by adopting a model of a rectangular rock body that causes induced earthquakes.

The input is the water injection energy E_i, and the outputs are the earthquake energy E_s of induced earthquakes, the friction energy E_f of the slip surface, the energy of water pressure compressing the rock body E_d, and the pressure loss energy E_p of water through the fracture. In addition, the thickness of the rock body was taken as the average value of the natural fracture spacing data, the ratio of width and length to the thickness, the friction coefficient of the slip surface of the rock body, and the fracture opening height were adopted as parameters.

Using hydraulic fracturing data from the Soultz, Cooper Basin, Basel, and Pohang sites, the earthquake energy was estimated using the Gutenberg-Richter magnitude distribution law, and it was shown that the energy balance is approximately valid. The ratio of the earthquake energy E_s to the water injection energy E_i is found to be a few percent. However, the ratio of $E_s+E_f+E_d+E_p$ to the injection energy E_i varied significantly from 0.1 to 0.9, depending on the value of the parameters. It was found that the optimal values of the parameters needed to be set at different sites.

It is useful to clarify the energy balance of hydraulic fracturing for the selection of the power plant construction site and setting of hydraulic fracturing conditions.

1. INTRODUCTION

The magnitude of induced earthquakes is determined by the pressure and flow rate of the injected water and by the subsurface structure during hydraulic fracturing conducted to develop EGS. We found that the magnitude of induced earthquakes has a strong relationship with the natural fracture density of the subsurface and reported the importance of analyzing the energy balance of hydraulic fracturing (Ishikawa and Yamada, 2019).

There is a report that calculates the energy balance for laboratory experiments (Goodfellow et al., 2015), and the earthquake energy was shown to be a few percent of the water injection energy, but it differs from the actual conditions for hydraulic fracturing. The total earthquake energy, water injection energy, and deformation moment of the experiments in Rustrel and Tournemire were calculated and it was pointed out that it was necessary to consider the fault structures, and the frictional and hydromechanical characteristics (De Barros et al., 2019). The energy of the injected water causes structural changes of the subsurface and is converted into earthquake and thermal energy, but the breakdown of this energy is not clarified.

We adopted a model in which the rock body that causes induced earthquakes was a rectangular body and its size was determined by the average value of natural fracture spacings in this report. We used data from hydraulic fracturing (Soultz, Cooper Basin, Basel, and Pohang), where relatively large earthquakes have occurred, to calculate the input and output energy in detail and to determine the energy balance. Furthermore, we selected parameters that were considered important for energy calculations and quantified their effects.

2. CALCULATION OF THE ENERGY BALANCE OF HYDRAULIC FRACTURING

The input is the water injection energy E_i calculated by the pressure and volume of the injected water, and the outputs are earthquake energy, friction energy, deformation energy, and pressure drop energy.

2.1 Water Injection Energy E_i

The water injection energy E_i(J) is expressed as the product of the wellhead pressure P(Pa), flow rate F(m^3/s), and time t(s) (Yamada and Ishikawa, 2017) and was calculated by equation (1).

$$E_i = P \cdot F \cdot t \tag{1}$$

2.2 Total earthquake energy E_s

The earthquake energy is caused by the generation of the slip in the rock body due to injection water. The vibrations caused by the slip propagate radially and the waveform of the vibrations can be measured by a seismograph. The earthquake energy E_{sM}(J) of magnitude M was calculated using the Gutenberg-Richter equation shown in equation (2) (Gutenberg and Richter, 1956).

$$\log(E_{sM}) = 1.5M + 4.8 \tag{2}$$

Since earthquake energies below M1.0 are negligibly small, earthquakes above M1.0 were used for the calculation. The magnitude of induced earthquakes is shown in the literature, together with the wellhead pressure and injection water flow rate, but the lower limit of the magnitude differs in the literature. Based on the magnitude and number of induced earthquakes shown in the literature, the approximation equation of the Gutenberg-Richter distribution equation was developed to obtain the number of earthquakes with a magnitude of M1.0 or greater. From the earthquake energy E_{sM} of magnitude M and the number of earthquakes N_M, the total earthquake energy E_s was calculated by equation (3).

$$E_s = \sum(E_{sM} \cdot N_M) \tag{3}$$

2.3 Total friction energy E_f

The friction energy is generated on the slip surface of the rock body. It is assumed that the induced earthquake is caused by the slip of a rectangular rock body of width X(m), length Y(m), and height Z(m) (Figure 1).

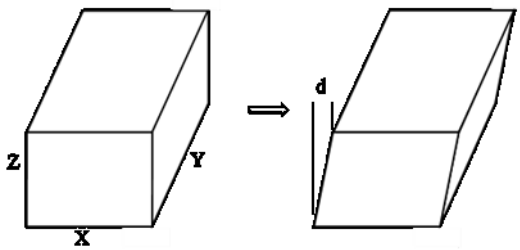

Figure 1: Slip of rock body

The height Z of a rock body can be expressed as the inverse of the natural fracture density D(/m). The width X and length Y are assumed to be integer multiples of Z.

If the depth of the hydraulic fracturing is D_h(m), the hydrostatic pressure P_w(Pa), the average rock body density from the surface to the depth of hydraulic fracturing is 2,500 kg/m^3, the wellhead pressure of hydraulic fracturing P(Pa), and the coefficient of friction f, then the friction force F_f is given by equation (4).

$$F_f = (2500D_h \times 9.8 - P_w - P) \cdot A \cdot f \tag{4}$$

The depth of induced earthquakes has a certain width around the hydraulic fracturing depth, but we assume that the depth of induced earthquakes is the same as the hydraulic fracturing depth.

The friction energy E_{fM}(J) due to an earthquake of magnitude M was calculated by equation (5).

$$E_{fM} = F_f \cdot d \tag{5}$$

Since both the earthquake energy E_{sM} in equation (2) and the friction energy E_{fM} in equation (5) are calculated from the magnitude M, the total friction energy E_f is calculated using the earthquake and the friction energies by equation (6).

$$E_f = E_s \times \frac{E_{fM}}{E_{sM}} \tag{6}$$

2.4 Total deformation energy E_d

This is the energy required to compress the rock body due to the increase in underground hydrostatic pressure caused by the injection of high-pressure water.

If the elasticity modulus of the granite is E(Pa) and the Poisson's ratio is ν, the bulk modulus K(Pa) can be expressed by equation (7).

$$K = \frac{E}{3(1-2\nu)} \tag{7}$$

Letting the rock volume be V_R(m^3), the compressed volume, ΔV(m^3), is given by equation (8).

$$\Delta V = V_R \times \frac{P}{K} \tag{8}$$

The deformation energy E_{dR}(J) of a single rock body is obtained by integrating ΔV with the wellhead pressure P by equation (9).

$$E_{dR} = \int \Delta V dP = \frac{V_R \times P^2}{2K} \tag{9}$$

Assuming that the number of rock bodies is equal to the total number N of earthquakes above M1.0, the total deformation energy E_d is calculated from E_{dR} and N by equation (10).

$$E_d = E_{dR} \cdot N \tag{10}$$

The fracture aperture height increases due to the change in thickness of the rock body caused by compression. The change in thickness of the rock body, ΔZ, can be expressed by equation (11).

$$\Delta z = z \times \frac{P}{K} \times \frac{1}{3} \tag{11}$$

2.5 Total pressure drop energy E_p

The pressure drop energy is the pressure loss energy of water passing through natural fractures in a rock body. Expressing the total pressure drop energy in E_p(J), the energy conservation equation for water is expressed by equation (12).

$$\frac{1}{2}mv_1^2 + \frac{m}{\rho}P_1 + mgz_1 = \frac{1}{2}mv_2^2 + \frac{m}{\rho}P_2 + mgz_2 + E_p \tag{12}$$

To evaluate the total pressure drop energy, let $v_1 = v_2$ and $z_1 = z_2$, and replace m/ρ with V to obtain equation (13).

$$E_p = V(P_1 - P_2) \tag{13}$$

By finding the total water injection volume V(m^3) and the pressure loss P_1-P_2(Pa), the pressure drop energy can be calculated. Since the total water injection volume V is the product of the flow rate F and the time t, it is calculated by equation (14).

$$V = F \cdot t \tag{14}$$

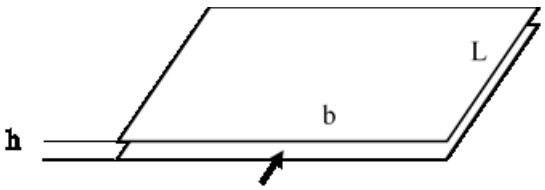

Figure 2: Pipe resistance of parallel plates

The fractures are considered as passages between parallel plates as shown in Figure 2, and the pressure loss is calculated from equations (15) and (16) of the pipe resistance.

$$P_1 - P_2 = Q \cdot R \tag{15}$$

$$R = \frac{12\mu L}{bh^3} \tag{16}$$

where Q, μ, L, b, h are flow rate (m^3/s), water viscosity (Pa*s), fracture length (m), fracture width (m), and fracture height (m) respectively.

The height of the fracture aperture, h, is the initial height, h_0, plus the change in thickness of the rock body due to compression, ΔZ.

2.6 Rupture Energy E_r

Rupture energy E_r is the energy to destroy the walls of a closed space in a rock body by increasing hydrostatic pressure. Because the size of the wall is not known, the rupture energy is not included in this report, although the closed space exists.

2.7 Lost Energy E_l

The lost energy E_l is due to the dissipation of the injected water. However, the dissipation of the injected water is considered to be small, and it is difficult to estimate the dissipation, so the lost energy is not included in this report.

In summary, the energy balance equation is shown in equation (17).

$$E_i = E_s + E_f + E_d + E_p \tag{17}$$

3. HYDRAULIC FRACTURING CONDITIONS

Four sites, Soultz, Cooper Basin, Basel, and Pohang, were selected and their main hydraulic fracturing conditions and timing of earthquake occurrence are listed in Table 1 (Schoenball and Kohl, 2013) (Kaieda et al., 2010) (Häring et al., 2008) (Yeo et al., 2020).

Table 1. Hydraulic fracturing conditions in four sites

	Soultz	Cooper Basin	Basel	Pohang 1-3
Period of Hydraulic Fracturing	2000 June	2003 Nov	2006 Dec	2016 Jan – 2017 Apr
Depth (m)	5,100	4,400	5,000	4,300
Underground Temperature (C)	150	250	190	145
Natural Fracture Density (/m)	0.6	0.15	0.3	9.7
Total volume of injected water (m^3)	23,095	14,852	11,393	9,342
Maximum Flow Rate (m^3/s)	0.05	0.024	0.053	0.039
Average Flow Rate (m^3/s)	0.045	0.019	0.028	0.020
Maximum Wellhead Pressure (MPa)	14	64	29	87
Average Wellhead Pressure (MPa)	13	58	19	69
Maximum Magnitude of Earthquake	2.6	3.7	3.4	3.2
Period from Injection Stop to Largest Earthquake (hr)	240	8	5	20

The first through fifth hydraulic fracturing was carried out at Pohang between January 2016 and September 2017. A large M5.5 earthquake occurred in November 2017 after hydraulic fracturing. Because the earthquake energy was greater than the water injection energy, hydraulic fracturing from January 2016 to April 2017 was included in this study.

4. CALCULATION RESULTS

4-1. Water injection energy

Table 2 shows the results of the water injection energy E_i calculated from the published hydraulic fracturing data.

Table 2. Water injection energy

	Soultz	Cooper Basin	Basel	Pohang 1-3
Water injection energy E_i (GJ)	300	879	288	515

4-2. Total earthquake energy

In order to ensure the same conditions for four sites, we used the Gutenberg-Richter distribution equation $\log(N_c)=a-bM$, and the total earthquake energy was calculated from this approximation by finding the number of earthquakes of magnitude greater than M1.0.

Figure 3's (1)-(4) shows the measured magnitude and cumulative number of earthquakes (black) and the value based on the approximation formula (red) at four sites.

Table 3 shows the number and magnitude of induced earthquakes observed at the four sites, and the sum of earthquake energy calculated from them. The number of earthquakes of M1.0 or greater and the sum of earthquake energy E_s calculated by the Gutenberg-Richter distribution approximation formula, and the ratio of E_s/E_i are also shown in Table 3.

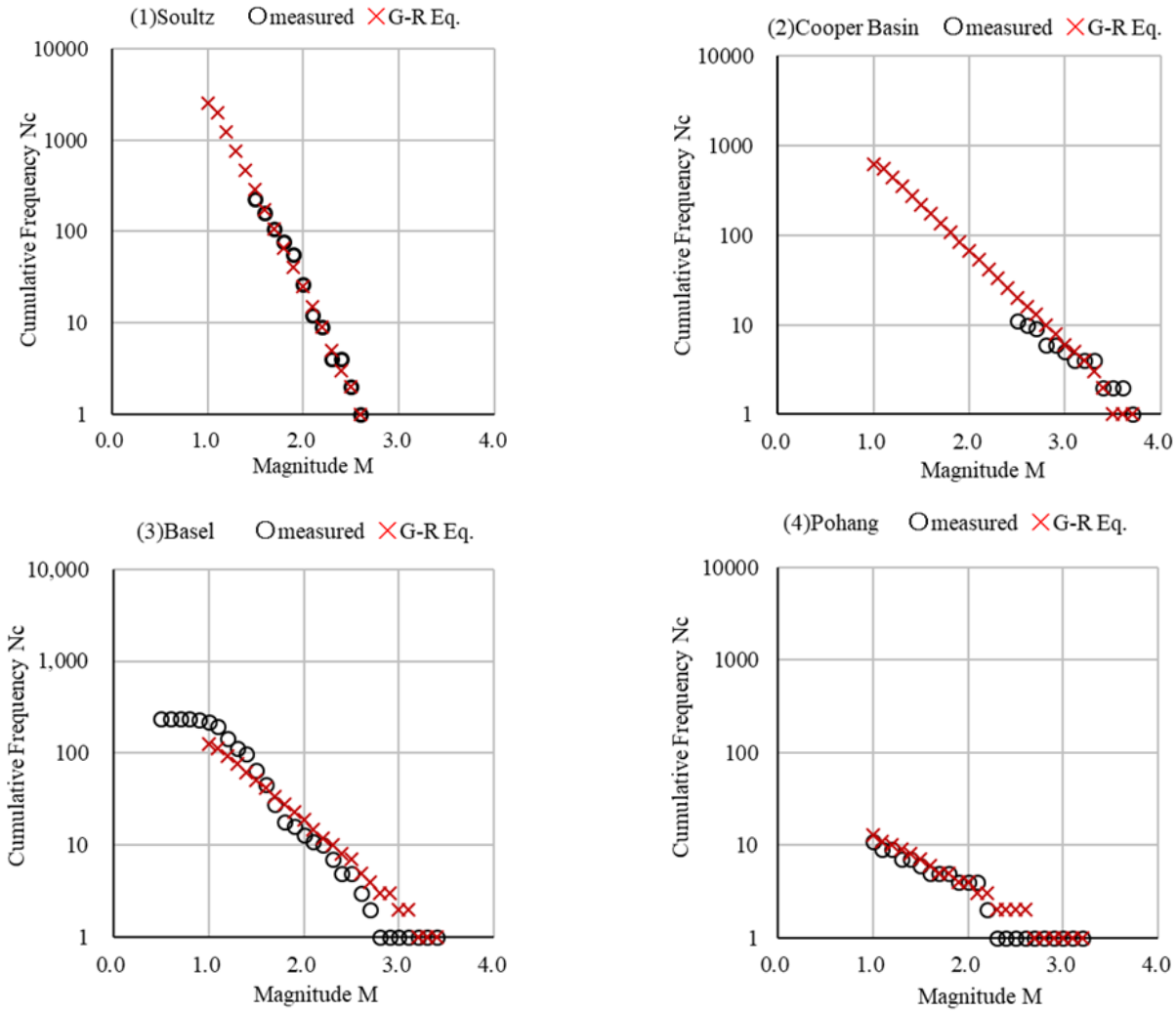

Figure 3. Magnitude and cumulative number of earthquakes based on measurement and the Gutenberg-Richter distribution approximation

Table 3: Total earthquake energy from the distribution approximation equation

	Soultz	Cooper Basin	Basel	Pohang 1-3
Observed number of induced earthquakes	221	11	239	32
Observed magnitude range	M1.5 – M2.6	M2.5 – M3.7	M0.5 – M3.4	M0.5 – M3.2
Sum of earthquake energy (GJ)	7.3	55.9	12.4	4.4
Coefficient a in approximation formula	5.5	3.82	2.92	1.6
Coefficient b in approximation formula	2.1	1.02	0.86	0.5
Number of >M1.0 earthquakes	2511	630	125	13
Total earthquake energy E_s (GJ)	16.0	65.2	16.5	4.8
Ratio E_s/E_i	0.05	0.07	0.06	0.01

4-3. Total friction energy, total deformation energy, total pressure drop energy

The total friction energy E_f, total deformation energy E_d, and total pressure drop energy E_p were calculated using the ratio of the width X and length Y of the rock body to the height Z, the coefficient of friction of the slip surface, and the initial height of the fracture aperture as parameters. The friction coefficient is about 0.6 according to Byerlee's raw, but it is lower when there exists pore water (Kanamori and Rivera, 2006). The friction coefficient was set 0.1 to 0.3.

Table 4 shows the total friction energy E_f, the total deformation energy E_d, the total pressure drop energy E_p, and the value of $(E_s+E_f+E_d+E_p)/E_i$.

Table 4. Calculation results

Parameters: x=y=5z, f=0.1, h_0 = 0.0001m				
	Soultz	Cooper Basin	Basel	Pohang 1-3
Total earthquake energy E_s (GJ)	16	65	17	5
Total friction energy E_f (GJ)	56	29	51	0
Total deformation energy E_d (GJ)	1	327	1	0
Total pressure drop energy E_p (GJ)	35	0	1	54
$E_s+E_f+E_d+E_p$ (GJ)	108	421	69	59
$(E_s+E_f+E_d+E_p)/E_i$	0.36	0.48	0.24	0.11

Parameters: x=y=7z, f=0.3, h_0 = 0.0001m				
	Soultz	Cooper Basin	Basel	Pohang 1-3
Total earthquake energy E_s (GJ)	16	65	17	5
Total friction energy E_f (GJ)	169	87	154	0
Total deformation energy E_d (GJ)	2	641	2	0
Total pressure drop energy E_p (GJ)	35	0	1	54
$E_s+E_f+E_d+E_p$ (GJ)	222	793	172	59
$(E_s+E_f+E_d+E_p)/E_i$	0.74	0.90	0.60	0.11

Parameters: x=y=5z, f=0.3, h_0 = 0.0m				
	Soultz	Cooper Basin	Basel	Pohang 1-3
Total earthquake energy E_s (GJ)	16	65	17	5
Total friction energy E_f (GJ)	169	87	154	0
Total deformation energy E_d (GJ)	1	327	1	0
Total pressure drop energy E_p (GJ)	82	0	1	442
$E_s+E_f+E_d+E_p$ (GJ)	268	479	172	446
$(E_s+E_f+E_d+E_p)/E_i$	0.89	0.54	0.60	0.87

5. DISCUSSION

The ratio of the total earthquake energy E_s to the water injection energy E_i ranged from 0.01 to 0.07 shown in Table 3.

From the calculation results in Table 4, the deformation energy was larger than the other energies in Cooper Basin because the height of the rock body was higher when the natural fracture density was lower. As the height of the rock body at Pohang was low, the change in the height due to hydrostatic pressure increase was small. When the height of the fracture aperture did not increase, the pressure drop energy was larger.

The ratio of $E_s+E_f+E_d+E_p$ to the water injection energy E_i was 0.90 depending on the values of parameters. This ratio close to 1 indicates that the energy balance is achieved. However, this ratio decreased to 0.11 depending on the values of parameters. It is necessary to set the optimum value of parameters for each site as a future task.

Induced earthquakes with the maximum magnitude occurred 5 hours to 10 days after the stop of water injection at the four sites discussed here as shown in Table 1. The subsurface stress increases by water injection and induces earthquakes. It took some time for the subsurface stress to induce the large earthquake. The difference in the time length is considered to be due to the difference in the subsurface structures. We have shown in this paper that the magnitude of induced earthquakes can be estimated by analyzing the energy balance over the period of hydraulic fracturing and aftershocks, but it is important to investigate and analyze the subsurface stresses to estimate the timing of induced earthquakes.

6. CONCLUSION

The balance between input and output is roughly established by calculating energies, assuming that the input energy is the water injection energy and the output energy is the total earthquake energy, total friction energy, total deformation energy, and pressure loss energy, and using three parameters, the ratio of the rock body size, the friction coefficient, and the fracture aperture height. This method is not limited to EGS, but is also valid for other fields such as shale gas and CCS.

It is important to analyze the relationship between water injection energy and subsurface stress of rock body because the induced earthquakes with the maximum magnitude occurred some time after the stop of water injection.

REFERENCES

De Barros, L., Cappa, F., Guglielmi, Y., Duboeuf, L. and Grasso, J. R.: Energy of Injection-induced Seismicity Predicted from In-situ Experiments, Scientific Reports, (2019).

Geoscience Australia, Earthquake Database, http://www.ga.gov.au/earthquakes/searchQuake.do, web access 27 July 2020.

Goodfellow, S.D., Nasseri, M. H.B., Maxwell, S. C. and Young, R. P.: Hydraulic fracture energy budget: Insights from the laboratory, Geophys. Res. Lett., 42, (2015).

Gutenberg, B. and Richter, C.F.: Magnitude and energy of earthquakes. Annali di Geofisica, 9, (1956).

Häring, M.O., Schanz, U., Ladner, F. and Dyer, B.C.: Charcterisation of the Basel 1 enhanced geothermal system, Geothermics, 37, (2008).

Ishikawa, T. and Yamada K.: Induced Earthquakes by Hot Dry Rock Power Generation: Influence of Injection Energy and Underground Structure, Proc. 43rd Workshop on Geothermal Reservoir Engineering, Stanford, (2019).

Kaieda, H., Sasaki, S. and Wyborn, D.: Comparison of Characteristics of Micro-Earthquakes Observed During Hydraulic Stimulation Operations in Ogachi, Hijiori and Cooper Basin HDR Projects, Proceedings World Geothermal Congress, (2010).

Kanamori, H. and Rivera, L.: Energy Partitioning During an Earthquake, Earthquakes: Radiated Energy and the Physics of Faulting Geophysical Monograph Series, 170, (2006).

Schoenball, M. and Kohl, T.: The Peculiar Shut-In Behavior of the Well GPK2 at Soultz-sous-Forets, GRC Transactions, 37, (2013).

Yamada, K. and Ishikawa, T.: Quantitative Analysis of Earthquake Energy Induced by Water Injection for Hot Dry Rock Power Generation, Proc. 39th New Zealand Geothermal Workshop, (2017).

Yeo, I.W., Brown, M.R., Ge, S. and Lee, K.K.: Causal Mechanism of Injection-induced Earthquakes through the Mw 5.5 Pohang Earthquake Case Study, Nature Communications, https://doi.org/10.1038/s41467-020-16408-0, (2020).